An Increase in Side Chain Entropy Facilitates Effector Binding: NMR Characterization of the Side Chain Methyl Group Dynamics in Cdc42Hs†

Adrienne P. Loh,‡ Norma Pawley,§ Linda K. Nicholson,§ and Robert E. Oswald*,‖

Department of Chemistry, University of Wisconsin-La Crosse, La Crosse, Wisconsin 54601, Department of Molecular Biology and Genetics, Cornell University, Ithaca, New York 14850, and Department of Molecular Medicine, Cornell University, Ithaca, New York 14850

Received October 17, 2000; Revised Manuscript Received January 17, 2001

ABSTRACT: Cdc42Hs is a signal transduction protein that is involved in cytoskeletal growth and organization. We describe here the methyl side chain dynamics of three forms of $^{2}H,^{13}C,^{15}N$-Cdc42Hs [GDP-bound (inactive), GMPPCP-bound (active), and GMPPCP/PBD46-bound (effector-bound)] from ^{13}C-^{1}H NMR measurements of deuterium T_1 and $T_{1\rho}$ relaxation times. A wide variation in flexibility was observed throughout the protein, with methyl axis order parameters (S^2_{axis}) ranging from 0.2 to 0.4 (highly disordered) in regions near the PBD46 binding site to 0.8−1.0 (highly ordered) in some helices. The side chain dynamics of the GDP and GMPPCP forms are similar, with methyl groups on the PBD46 binding surface experiencing significantly greater mobility (lower S^2_{axis}) than those not on the binding surface. Binding of PBD46 results in a significant increase in the disorder and a corresponding increase in entropy for the majority of methyl groups. Many of the methyl groups that experience an increase in mobility are found in residues that are not part of the PBD46 binding interface. This entropy gain represents a favorable contribution to the overall entropy of effector binding and partially offsets unfavorable entropy losses such as those that occur in the backbone.

Highly specific protein−protein and protein−small molecule interactions are the basis for a wide variety of biological processes. While the role of structure in molecular recognition is well recognized, the role of dynamics is less well understood. Many proteins function by binding ligands using a lock-and-key mechanism. However, some proteins such as the Ras-like GTPases are capable of interacting with a variety of different effector and regulator proteins using the same binding surface (*1*−*6*). This suggests that some proteins must have binding regions that are able to adjust to a variety of different incoming ligands. Indeed, recent experiments have indicated that protein flexibility is critical for function (*7*−*10*) and that binding of protein ligands can have significant effects on the order (or disorder) of the protein (*11*−*14*). The particular way in which dynamic motions contribute to the free energy of binding for a given protein is a topic of great interest (*15*−*18*). We have previously characterized the backbone dynamics of three functionally different forms of the GTPase Cdc42Hs using ^{15}N-^{1}H NMR spectroscopy and found that activation of Cdc42Hs has little effect on the backbone dynamics, while ligand binding results in a significant decrease in the complexity of the backbone dynamics (*19*). Here we present an analysis of the dynamics of the side chain methyl groups in the same forms of Cdc42Hs using ^{13}C-^{1}H NMR spectroscopy and discuss the results in terms of the entropic contributions from side chain motions to the free energies of protein activation and ligand binding.

Cdc42Hs is a member of the Ras superfamily of GTP-binding proteins, a group of signal transduction proteins that are involved in a diverse variety of biological processes including cell growth, differentiation, cytoskeletal organization, protein trafficking, and secretion (*20*). Members of this family are activated by the exchange of GDP[1] for GTP and are inactivated by the intrinsic enzymatic hydrolysis of GTP to GDP by the protein. Cdc42Hs in particular interacts with a variety of proteins that serve to regulate its activity (regulators) and transmit the signals sent by an activated Cdc42Hs molecule (effectors). The majority of the interactions between Cdc42Hs and its regulator and/or effector proteins occur at three main sites: switch I, switch II, and the insert region (Figure 1). The switch I and switch II regions have relatively flexible backbones and have been

† This work was supported by a grant from the National Institutes of Health: R01 GM56233.

* To whom correspondence should be addressed: Department of Molecular Medicine, College of Veterinary Medicine, Cornell University, Ithaca, NY 14853; phone: 1-607-253-3877; fax: 1-607-253-3659; E-mail: reo1@cornell.edu.

‡ University of Wisconsin-La Crosse.

§ Department of Molecular Biology and Genetics, Cornell University.

‖ Department of Molecular Medicine, Cornell University.

[1] Abbreviations: GDP: guanosine-5′-diphosphate; GTP: guanosine-5′-triphosphate; GMPPCP: β,γ-methylene derivative of GTP; PAK: p21-activated kinase; PBD46: 46 amino acid portion of the Cdc42Hs binding domain on PAK; switch I: residues 31−40 on Cdc42Hs; switch II: residues 57−74 on Cdc42Hs; insert region: residues 118−134 on Cdc42Hs; HSQC: heteronuclear single quantum correlation; NMR: nuclear magnetic resonance; NOE: nuclear Overhauser effect; T_1: longitudinal relaxation time; T_2: transverse relaxation time; $T_{1\rho}$: transverse relaxation time in the rotating frame; S^2: generalized order parameter; S^2_{axis}: order parameter for the methyl group symmetry axis; τ_e: local correlation time; τ_m: molecular or global correlation time, GDI: guanidine nucleotide dissociation inhibitor; GAP: GTPase activating protein.

10.1021/bi002418f CCC: $20.00
Published on Web 03/20/2001

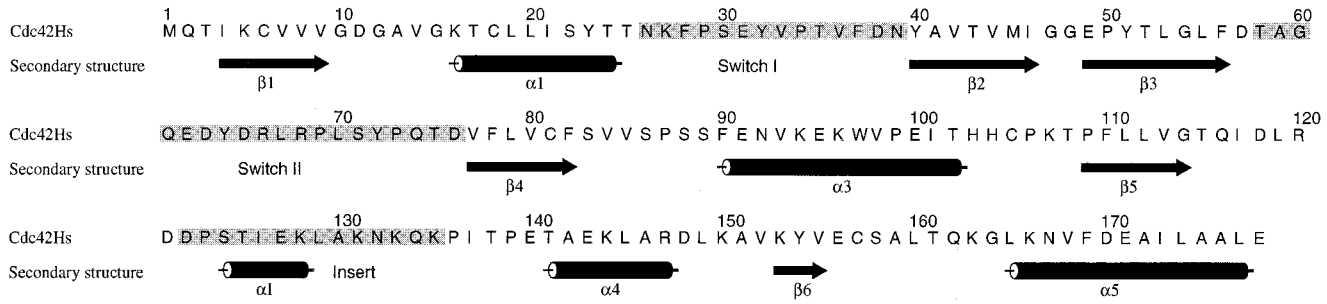

FIGURE 1: Amino acid sequence of Cdc42Hs. The secondary structure components determined from the NMR structure of Cdc42Hs-GDP are also indicated (*26*). [This figure was produced using the program ALSCRIPT (*56*)]

shown to exhibit varying degrees of disorder in NMR and X-ray studies (*4*, *19*, *21*−*25*). The insert region is predominantly structured and contains a mobile α-helix (*19*, *22*, *25*, *26*). One of the effectors for Cdc42Hs is p21-activated serine/threonine kinase (PAK). We have previously used a 46-residue peptide fragment of PAK (PBD46) to show that the switch I and switch II regions of Cdc42Hs are involved in PAK binding (*4*, *21*) and have solved the solution structures of the inactive (Cdc42Hs-GDP) and the active, peptide-bound (Cdc42Hs-PBD46) forms of Cdc42Hs using NMR spectroscopy (*21*, *26*).

EXPERIMENTAL PROCEDURES

Protein Preparation and Purification. The details of cell growth and protein purification have been described previously (*4*, *21*). Briefly, uniformly ^{15}N-enriched Cdc42Hs was expressed as a hexa-histidine-tagged protein in *Escherichia coli* strain BL21(DE3) from pET-15b-Cdc42Hs. $^{15}NH_4Cl$ and ^{13}C-glucose were substituted for unlabeled compounds in M9 media. Partial deuteration (70%) was achieved following the procedure of Yamazaki et al. (*27*). The expression plasmid was subcloned to contain the N-terminal 178 amino acids (plus a glycine, serine, and histidine which occur before the starting methionine) from the original pGEX-Cdc42Hs expression plasmid to improve the yield and to remove the unstructured C-terminal tail. The amino acid sequence of Cdc42Hs is shown in Figure 1. The three functional regions of the protein have been identified as residues 31−40 (switch I), residues 57−74 (switch II), and residues 118−134 (insert).

Three forms of Cdc42Hs were examined: Cdc42Hs-GDP (Cdc42Hs bound to one molecule of GDP), Cdc42Hs-GMPPCP (Cdc42Hs bound to one molecule of GMPPCP, a non-hydrolyzable analogue of GTP), and Cdc42Hs-PBD46 (Cdc42Hs bound to one molecule of GMPPCP and one molecule of PBD46). The exchange of GDP for GMPPCP was performed as described in John et al. (*28*). To prepare Cdc42Hs-PBD46, PBD46 and Cdc42Hs-GMPPCP were mixed in equimolar concentrations and incubated overnight at 4 °C. The complex was then purified on a Sephacryl S-100 column equilibrated with NMR buffer (25 mM NaCl, 5 mM NaH_2PO_4, 5 mM $MgCl_2$, and 1 mM NaN_3) at pH* 5.5 (no correction for isotope effects). The PBD46 peptide has been previously shown to be in slow exchange with Cdc42Hs-GMPPCP and to bind with an affinity of 16 nM (*4*).

NMR Spectroscopy. Protein samples were prepared in NMR buffer with 10% D_2O at pH* 5.5 at the following concentrations: Cdc42Hs-GDP: 0.8 mM; Cdc42Hs-GMPPCP: 1.0 mM; Cdc42Hs-PBD46: 1.0 mM (*4*, *26*). ^{13}C-^{1}H HSQC spectra were obtained at 25 °C on a Varian Inova 600 MHz spectrometer equipped with a triple resonance pulsed-field gradient probe, using the pulse schemes described in Muhandiram et al. (*29*). Chemical shifts were referenced as described previously (*26*). Values for the mixed spin relaxation times $T_1(I_zC_zD_z)$ and $T_1(I_zC_z)$ were obtained by measuring nine spectra each with delays of 0.05, 4.5, 9.5 (in duplicate), 15, 21, 28 (in duplicate), 36, 45, and 57.7 ms. Values of the mixed spin relaxation time $T_{1\rho}(I_zC_zD_y)$ were obtained by measuring eight spectra with delays of 0.20, 1.3 (in duplicate), 2.8, 4.4 (in duplicate), 6.2, 8.4, 10.9, and 15.1 ms. All data sets were recorded using 160 × 512 real data points at 16 scans per point, with quadrature obtained in t_1 using States-TPPI (*30*). The ^{2}H lock receiver was disabled during the periods of deuterium decoupling in the pulse schemes.

Data Analysis. Spectra were processed using NMRPipe v. 1.6 (*31*) on a Sun Ultra 5 workstation. Data were zero-filled to double the original number of data points and apodized with a mixed exponential-Gauss window function. In all cases, numerical solvent suppression was applied prior to Fourier transformation, and baseline correction was applied after Fourier transformation. Spectra were visualized and peak-picked using the PIPP suite of assignment programs (*32*). Peak volumes were determined by fitting a Gaussian line shape to the experimental peak using the program nlinLS (F. Delaglio, NIH). Mixed spin relaxation times [$T_1(I_zC_zD_z)$, $T_1(I_zC_z)$, or $T_{1\rho}(I_zC_zD_y)$] were then obtained using conjugate gradient minimization and Monte Carlo simulation to fit the relaxation delay points to an exponential decay function with time constant T_i and zero intercept (*33*). Errors in relaxation times (expressed as standard deviations) were chosen as the larger of those from either the exponential fit or from a duplicate pair of relaxation delay points. Deuterium relaxation times (T_1 and $T_{1\rho}$) were then obtained from the mixed spin relaxation times using eqs 1 and 2 (*29*).

$$\frac{1}{T_1(D)} = \frac{1}{T_1(I_zC_zD_z)} - \frac{1}{T_1(I_zC_z)} \quad (1)$$

$$\frac{1}{T_{1\rho}(D)} = \frac{1}{T_{1\rho}(I_zC_zD_y)} - \frac{1}{T_1(I_zC_z)} \quad (2)$$

Values for the dynamics parameters S^2 and τ_e for each deuteron were obtained by fitting the deuterium relaxation times to the simple, Lipari−Szabo model-free spectral density function for isotropic molecular tumbling (*34*, *35*),

$$J(\omega) = \frac{2}{5}\left[\frac{S^2\tau_m}{1+(\omega\tau_m)^2} + \frac{(1-S^2)\tau}{1+(\omega\tau)^2}\right] \quad (3)$$

where $\tau = \tau_e\tau_m/(\tau_e + \tau_m)$, τ_m is the molecular correlation time, which characterizes the time scale of molecular tumbling, τ_e is the local correlation time, which characterizes the time scale of local motion ($\tau_e < \tau_m$), and S^2 is the $^{13}C-D$ bond axis order parameter, which describes the degree of restriction (or amplitude) of the local $^{13}C-D$ bond motions on the τ_e time scale. Methyl groups were assumed to have ideal tetrahedral geometry and to follow a three-site hop model of motion, whereupon the order parameter describing the methyl group symmetry axis, S^2_{axis}, can be calculated from S^2 by

$$S^2_{axis} = \frac{S^2}{(3\cos^2\theta - 1)^2/4} = \frac{S^2}{0.111} \quad (4)$$

using $\theta = 109.5°$ (*36*). The deuterium relaxation times can be related to the spectral density function through eqs 5 and 6 by assuming that the only significant mechanism of deuterium relaxation is quadrupolar (*37*),

$$\frac{1}{T_1} = \frac{3}{16}\left(\frac{e^2qQ}{\hbar}\right)^2[J(\omega_D) + 4J(2\omega_D)] \quad (5)$$

$$\frac{1}{T_{1\rho}} = \frac{3}{32}\left(\frac{e^2qQ}{\hbar}\right)^2[9J(0) + 15J(\omega_D) + 6J(2\omega_D)] \quad (6)$$

where $e^2qQ/\hbar$ is the quadrupole coupling constant [165 kHz for methyl deuterons (*38*)] and ω_D is the Larmor frequency of the ^2H nucleus. Isotropic values for τ_m were obtained from ^{15}N relaxation parameters as described previously (*19*). Values for S^2 and τ_e under the isotropic approximation were calculated from eqs 3, 5, and 6 using NORMAdyn (Pawley and Nicholson, Cornell University) for all methyl-containing residues for which experimental values of both T_1 and $T_{1\rho}$ were available.

To determine whether Cdc42Hs tumbles anisotropically, ^{15}N relaxation data (*19*) for the GDP[2] and PBD46 forms were fit to axially symmetric molecular tumbling models using anisotropic diffusion tensors obtained from the program R2R1_diffusion (*39*) and atomic coordinates from the NMR solution structures (*21*, *26*) or X-ray crystal structure (N. Nassar, G. Hoffman, and R. A. Cerione, personal communication). The diffusion tensor for each structure was determined using T_1 and T_2 values at 600 MHz for a subset of peaks obtained by filtering out those that had NOE values less than 0.65 and those displaying significant internal motion in the picosecond−nanosecond and microsecond−millisecond time scales (Wang, C., Pawley, N., and Nicholson, L. K., manuscript in preparation). The significance of the reduction in chi-squared relative to the isotropic case was tested using the F-statistic. In the cases where the axially symmetric diffusion tensors gave statistically significant reductions in chi-squared, values of S^2_{axis} (representing an average of the C−D bond vector orientations, i.e., the methyl rotor axis) and τ_e for side chain methyl groups were calculated using the program NORMAdyn (Pawley and Nicholson, Cornell University), under the assumption that the orientation of the methyl group axis is fast relative to the reorientation of the molecule. Solvent accessibilities were calculated using the program NACCESS (*40*).

Entropy Calculations. The contributions to the change in conformational entropy from side chain motions upon activation (GDP- vs GMPPCP-bound) or PBD46 binding (GMPPCP- vs GMPPCP/PBD46-bound) were estimated using the approximate relation presented by Yang and Kay (*16*):

$$\frac{S_p}{k} = A + \ln\pi[3 - (1 + 8S_{LZ})^{1/2}] \quad (7)$$

where S_p is the conformational entropy, S^2_{LZ} is the Lipari-Szabo order parameter (S^2_{axis}), k is the Boltzmann constant, and A is a constant that depends on the model used to describe the methyl axis motion, assuming all motions are independent and uncoupled. For a change in conformational entropy between states a and b, eq 7 reduces to

$$\Delta S = S_{p,b} - S_{p,a} = Nk\ln\left[\frac{3 - (1 + 8S_{LZ,b})^{1/2}}{3 - (1 + 8S_{LZ,a})^{1/2}}\right] \quad (8)$$

where ΔS is in units of kJ/mol and is independent of the value of A. The classical expression for the rotational partition function used to derive eq 7 is only valid for $S^2_{LZ} \leq 0.95$. Therefore, methyls with order parameters greater or equal to 0.95 were excluded, as were methyls with order parameters less than 0.05 (M1 only), as this portion of the S_p vs S^2_{LZ} curve is difficult to model. Changes in conformational entropy were then calculated using only those methyls for which assignments were available in both constructs. In total, 33 methyls in Cdc42Hs-GMPPCP and Cdc42Hs-PBD46 were compared for the entropy change due to PBD46 binding, and 38 methyls in Cdc42Hs-GDP and Cdc42Hs-GMPPCP were compared for the entropy change due to nucleotide exchange. Reported errors in ΔS arise solely from the propagated error in the order parameters through eq 8.

RESULTS

Determination of Methyl Symmetry Axis Order Parameters. The motions of partially deuterated methyl ($^{13}CDH_2$) side chains were studied in three forms of Cdc42Hs: inactive (Cdc42Hs-GDP), active (Cdc42Hs-GMPPCP), and bound to a fragment of the effector PAK (Cdc42Hs-PBD46). The relaxation of deuterons in all three forms was measured using ^{13}C-^1H NMR spectroscopy, as described by Muhandiram et al. (*29*). Sample ^{13}C-^1H HSQC spectra are shown in Figure 2. Assignments for the majority of the 115 methyl groups in Cdc42Hs (89 in Cdc42Hs-GDP, 88 in Cdc42Hs-GMPPCP, and 82 in Cdc42HS-PDB46) have been previously published (*4*, *21*, *26*). Values for deuterium T_1 and $T_{1\rho}$ relaxation times were obtained for 77, 78, and 72 of the assigned methyl deuterons in Cdc42Hs-GDP, -GMPPCP, and -PDB46, respectively (Figure 3). Methyl group mobilities were characterized by extracting values for the methyl group symmetry

[2] Cdc42Hs-GDP was used as an equivalent reference structure to Cdc42Hs-GMPPCP as no crystal structure of Cdc42Hs-GMPPCP is available. The side chain dynamics of both forms are shown in this paper to be very similar. The backbone dynamics of both forms have previously been shown to be very similar (*19*).

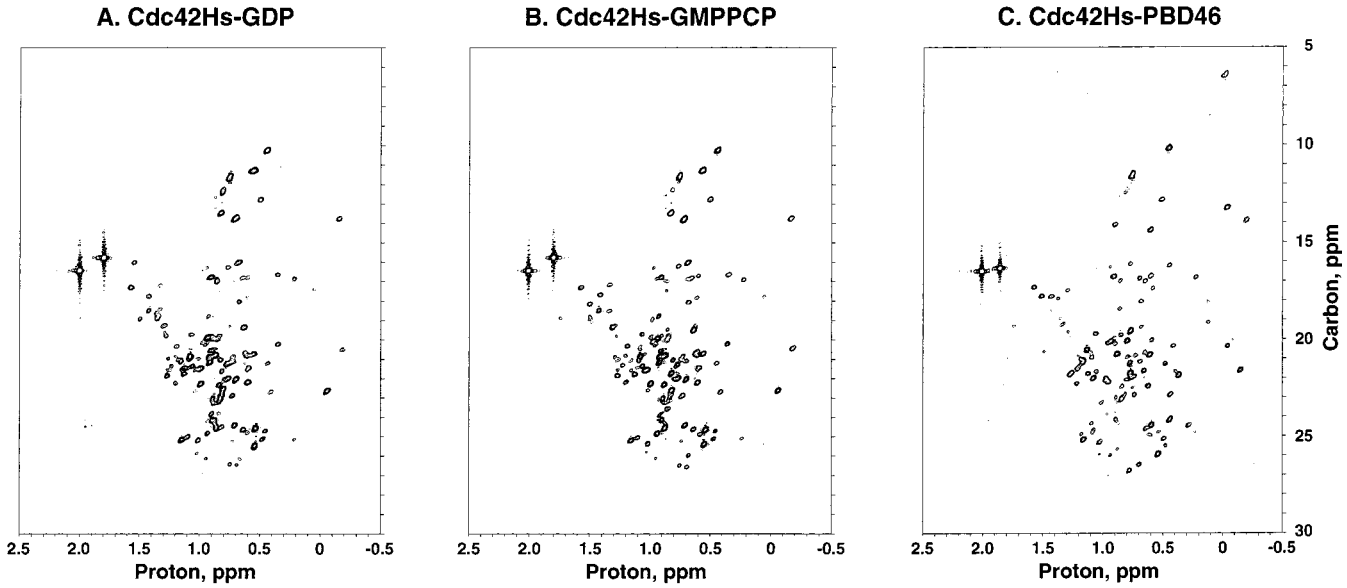

FIGURE 2: Sample ^{13}C-^{1}H HSQC (*57*) spectra of (A) Cdc42Hs-GDP, (B) Cdc42Hs-GMPPCP, and (C) Cdc42Hs-PBD46, obtained at 600 MHz using the $T_{1\rho}$ pulse sequence with a relaxation delay of 0.2 ms. Only Cdc42Hs is ^{13}C-labeled; therefore, PBD46 resonances do not appear in panel C.

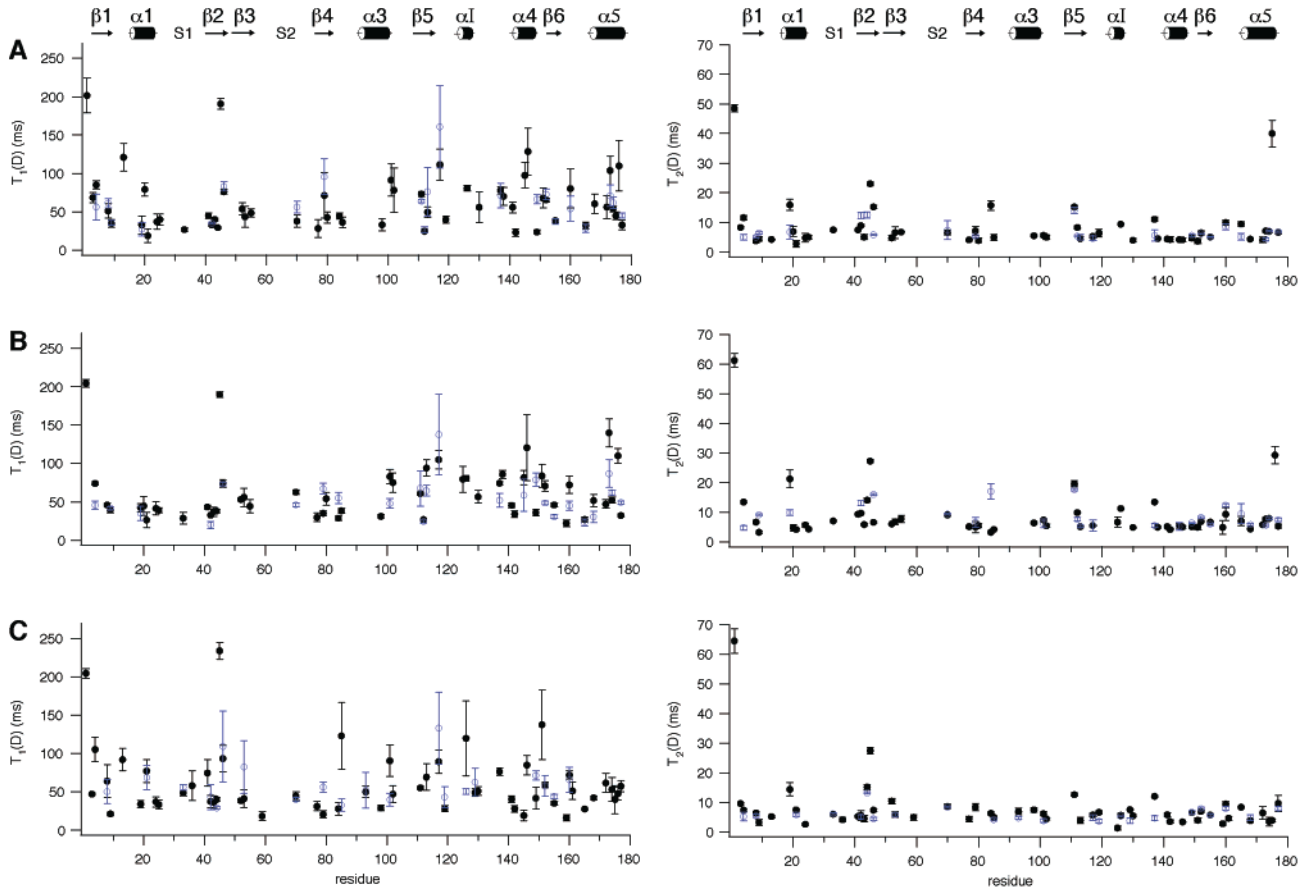

FIGURE 3: T_1 and T_2 relaxation times for side chain methyl deuterons in Cdc42Hs, calculated from eqs 1 and 2. The blue data points are used to distinguish the data for a second methyl group on the same residue. (A) Cdc42Hs-GDP, (B) Cdc42Hs-GMPPCP, and (C) Cdc42Hs-PBD46.

axis order parameter (S^2_{axis}) from the measured T_1 and $T_{1\rho}$ values using an isotropic molecular tumbling model. Order parameters can range in value from 1, which represents completely restricted motion (i.e., fixed orientation) to 0, which represents unrestricted motion. The time scale of this motion is characterized by the local correlation time, τ_e. In all three forms, τ_e was observed to range in value from ~10 to 100 ps (data not shown), with little correlation between the time scale of motion and structural elements or solvent accessibility.

Because the backbone dynamics of Cdc42Hs (*19*) are more complex (more time scales, more chemical exchange) in the GDP and GMPPCP forms than in the PBD46 form, we chose to reanalyze the backbone relaxation data of the forms for

Table 1: Average Symmetry Axis Order Parameters for Cdc42Hs[a]

averages[b]	GDP	GMPPCP	PBD46	GMPPCP − GDP	PBD46 -GMPPCP
All methyls	0.664 ± 0.036	0.665 ± 0.037	0.584 ± 0.030	−0.012 ± 0.021	−0.082 ± 0.037
At PBD46 interface[c]	0.571 ± 0.053 (27)	0.522 ± 0.056 (24)	0.530 ± 0.054 (27)	−0.009 ± 0.041 (21)	0.015 ± 0.063 (18)
Not at PBD46 interface	0.729 ± 0.047 (38)	0.748 ± 0.044 (41)	0.620 ± 0.033 (41)	−0.013 ± 0.022 (34)	−0.150 ± 0.040 (26)
Difference (interface-no interface)	0.158 ± 0.071	0.226 ± 0.071	0.090 ± 0.063	−0.004 ± 0.047	−0.165 ± 0.075

[a] Values in parentheses represent the number of methyl groups used to obtain the average. Values of S^2_{axis} were obtained using an isotropic molecular tumbling model. [b] All error limits are reported as standard deviations of the mean. [c] The interface is defined as being within 5 Å of the side chains on PBD46, as determined by the program SwissPBDView (*55*), http://www.expasy.ch/spdbv.

Table 2: Best Fits of Isotropic and Axially Symmetric Diffusion Tensors to ^{15}N Relaxation Data[a]

structure/ model	τ_m (ns)	$D_\parallel/D_\perp$	θ (rad)	ϕ (rad)	χ^2_{red} (DT)[b]	χ^2_{red} (MF4)[c]
GDP (143 aa)	14.8 ± 0.4[a]					
isotropic	14.6	1	0	0	28.3	28.7
NMR[d]	14.6	1.13	0.34	5.1	21.2	31.2
X-ray[e]	14.7	1.18	0.14	6.1	12.4	31.9
PBD46 (155 aa)	18.6 ± 0.5[a]					
isotropic	19.3	1	0	0	7.5	54.0
NMR[f]	19.1	1.14	1.1	6.3	6.2	67.7

[a] Relaxation data and optimized isotropic τ_m values are from Loh et al. (*19*). [b] Values from calculation of the diffusion tensor (DT) using only those residues that survive the filter as described in text. [c] Values from the fit of the relaxation data to the most appropriate local model for all residues, using the axially symmetric diffusion tensor indicated. The program ModelFree v.4 (MF4) (*39*) was used for these calculations. [d] Feltham et al. (*26*). [e] N. Nassar, G. Hoffman, and R. A. Cerione, personal communication. [f] Gizachew et al. (*21*).

which structures are available (GDP and PBD46) to be sure that an isotropic tumbling model is appropriate for Cdc42Hs. Axially symmetric diffusion tensors were constructed for Cdc42Hs-GDP based on (i) the NMR solution structure (*26*), $D_\parallel/D_\perp = 1.13$, and (ii) the X-ray crystal structure (N. Nassar, G. Hoffman, and R. A. Cerione, personal communication), $D_\parallel/D_\perp = 1.18$, and for Cdc42Hs-PBD46 based on the NMR structure (*21*), $D_\parallel/D_\perp = 1.14$ (Table 2). The decrease in the reduced chi-squared statistic upon introduction of an axially symmetric diffusion tensor was statistically significant only for Cdc42Hs-GDP. However, the use of either anisotropic diffusion tensor in modeling the entire set of Cdc42Hs-GDP ^{15}N relaxation data resulted in minimal changes in either the local model complexity or in the values of the backbone order parameters. This is in contrast to what was observed for proteins that have been best described using axially symmetric tumbling models such as human ubiquitin ($D_\parallel/D_\perp = 1.17$) (*41*), HIV-1 protease ($D_\parallel/D_\perp = 1.34$) (*42*) and trp repressor ($D_\parallel/D_\perp = 1.29$) (*43*). Furthermore, values for S^2_{axis} that were recalculated using the stereospecific assignments of the methyl groups of Cdc42Hs-GDP (*26*) and the axially symmetric diffusion tensor from the crystal structure differed little from those obtained using the isotropic tumbling model (Table 2). Therefore, the isotropic tumbling model appears to be appropriate for all forms of Cdc42Hs.

Activation of Cdc42Hs has Little Effect on Side chain Dynamics. Values for S^2_{axis} were reliably obtained for 65 (GDP-bound) and 64 (GMPPCP-bound) of the side chain methyl groups in Cdc42Hs (Figure 4, panels A and B). The side chain dynamics of the two forms were very similar over a wide range of mobilities, with S^2_{axis} values ranging from 0.009 to 1 in Cdc42Hs-GDP, and from 0.063 to 1 in Cdc42Hs-GMPPCP. The observed values of S^2_{axis} for a given amino acid type were generally found to be consistent with those observed for other proteins (*44*), although unusually low order parameters were found in a few cases [A175 (Cdc42Hs-GDP only), A176 (Cdc42Hs-GMPPCP only), A41, V42, V44, and V84]. Values of S^2_{axis} are displayed on the ribbon structures of Cdc42Hs-GDP and Cdc42Hs-GMPPCP in Figure 5, panels A and B.

The similarity of the side chain dynamics of the inactive and active forms is reflected in the almost identical average values of S^2_{axis} (0.66 ± 0.04, Table 1). Not surprisingly, the side chains are significantly more mobile than the backbone, for which the average order parameter was ∼0.95 in both forms (*19*). Particularly low side chain order is experienced at the C- and N-termini (M1; A175 in -GDP; A176 in -GMPPCP) and most of the residues in the surface-exposed β2 sheet (V42−I46). Regions of relatively high order include part of the α4 helix (T141−A146) and selected regions of the α1, α3, and α5 helices. Unfortunately, neither switch I nor switch II could be well characterized, as there are few methyl-bearing residues in these regions. However, a large number of residues that comprise the PBD46 binding surface contain methyl groups, including the β2 sheet, the C- and N-termini, and small portions of switch I and switch II (see shaded regions of Figure 4). In both forms, methyl groups on the binding surface experience significantly greater mobility (lower S^2_{axis}) than those not on the binding surface (Table 1). This pronounced difference is indicative of the importance of flexibility in achieving an induced fit to an incoming ligand and may be common to proteins such as Cdc42Hs that bind a variety of different ligands using the same binding site.

It is interesting to note that there are several isolated locations where methyl groups experience relatively low order parameters (L19, V84, L111, L112, I126, I137). Many of these residues are located in regions of the protein where the backbone is structured, and all of their methyls are buried to some extent (Figure 6): L19 is in the center of the α1 helix near the GDP/GTP binding pocket [relative solvent accessibility (rsa) = 3.9%], L111 and L112 are in the center of the β5 strand [rsa = 0% for both residues], I126 is in the middle of the insert helix facing inward (rsa = 20%), and I137 is at the end of the α4 helix (rsa = 1.1%), facing V84 (located in the loop at the end of α3; rsa = 5.4%). In fact, a small region of the backbone near V84 was found to exhibit chemical exchange dynamics (*19*). It has been suggested that this exchange might be due to a wagging motion of the insert helix with one side of the hinge close in space to that site. The localized high mobility of the interacting side chains of I137 and V84 reinforces this suggestion. In fact, V84 is one

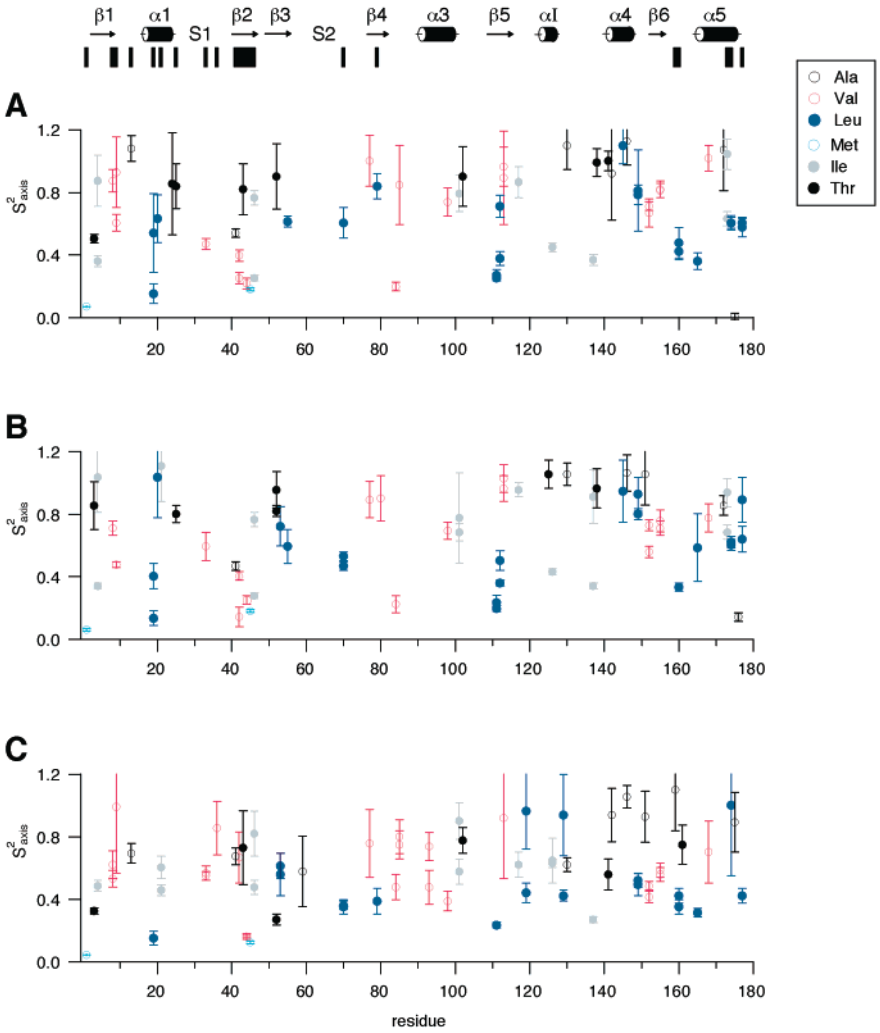

FIGURE 4: Symmetry axis order parameters for side chain methyl deuterons in Cdc42Hs, colored by residue type. Molecular correlation times were obtained from ^{15}N relaxation data as described in Loh et al. (*19*). (A) Cdc42Hs-GDP: $\tau_m = 14.8$ ns, (B) Cdc42Hs-GMPPCP: $\tau_m = 12.6$ ns, (C) Cdc42Hs-PBD46 $\tau_m = 18.6$ ns. The binding interface of PBD46 with Cdc42Hs methyl groups is indicated by black bars at the top of the figure.

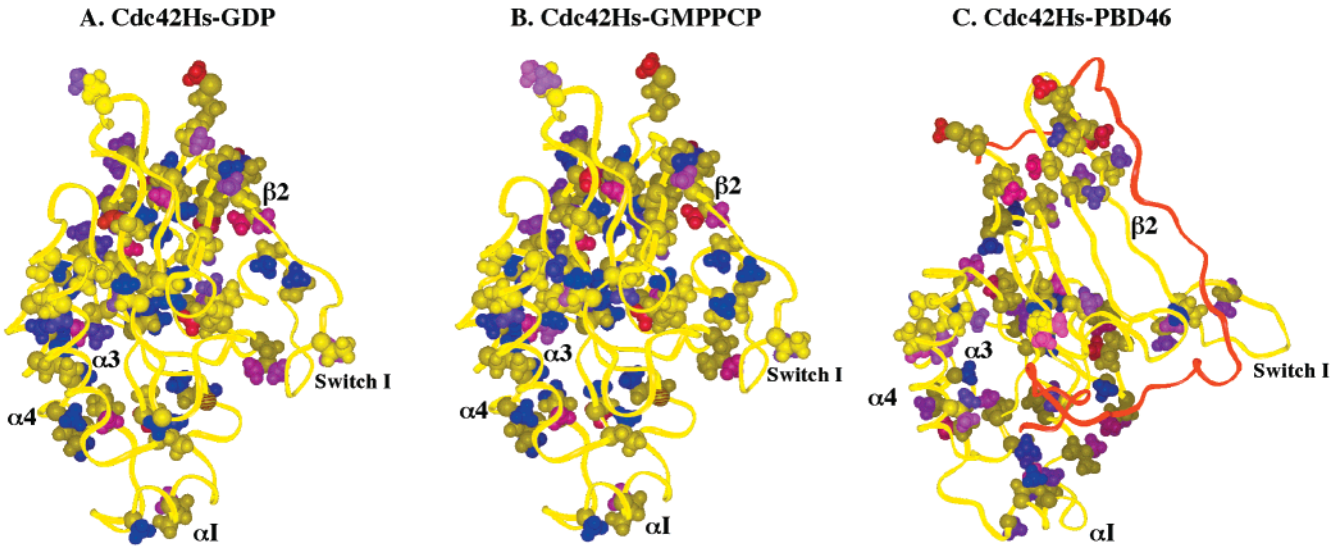

FIGURE 5: Ribbon diagram of the symmetry axis order parameters for side chain methyl deuterons in Cdc42Hs: (A) Cdc42Hs-GDP, (B) Cdc42Hs-GMPPCP, and (C) Cdc42Hs-PBD46. Values of S^2_{axis} are indicated by shades of blue that range from dark blue (1) to red (0). The PBD46 peptide backbone is shown in red.

of the few residues in Cdc42Hs that have S^2_{axis} values that are unusually low relative to those observed for valine methyls in other proteins (*44*). The general similarity of the side chain dynamics of the GDP and GMPPCP forms is illustrated in Figure 7, panel A, where the order parameters for the two forms are compared directly. Values of the

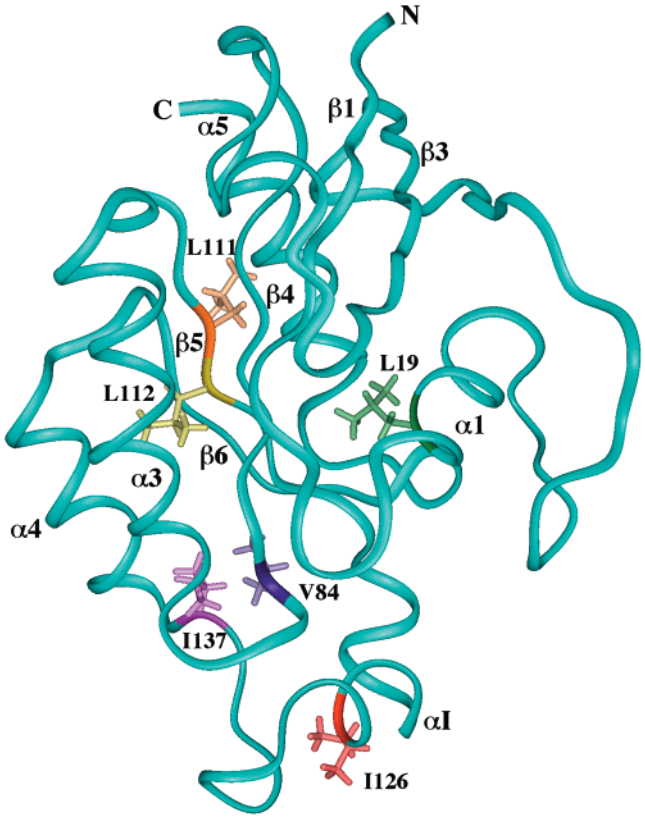

FIGURE 6: Ribbon structure of Cdc42Hs-GDP showing the methyl groups that experience increased mobility in isolated locations.

difference in methyl group order parameters ($\Delta S^2_{\text{axis, activation}}$) are well scattered about 0, both for residues at the binding interface and for residues away from the binding interface. The average difference between S^2_{axis} values for the two forms is also negligible for both groups of methyl groups (Table 1). Thus, as was observed in the backbone dynamics study (*19*), there is no significant change in the methyl side chain dynamics upon activation.

Binding of the PBD46 Ligand Increases Side Chain Mobility. Values for S^2_{axis} were reliably obtained for 68 of the methyl groups in the ligand-bound form of Cdc42Hs (Cdc42Hs-PBD46, Figure 4, panel C, and Figure 5, panel C). As with the GDP and GMPPCP forms, a wide range of order parameters is observed, the majority of which are comparable to those found for other proteins according to residue type (*44*). Only T52 (located at a surface exposed end of the β3 strand) and V44 (located in the surface exposed β2 strand) have order parameters that fall into the low end of their distributions.

In contrast to what was observed upon activation, the overall mobility of the side chain methyls increases upon ligand binding, as demonstrated by the decrease in the average value of S^2_{axis} from 0.66 ± 0.04 for the PBD46-free forms to 0.58 ± 0.03 for the PBD46-bound form (Table 1). The general increase in side chain mobility is more pronounced for residues away from the PBD46 binding interface (Figure 7, panel B), where $\Delta S^2_{\text{axis,bind}} = -0.15 \pm 0.04$ (as compared with -0.08 ± 0.04 for all methyls, Table 1). Not unexpectedly, the average change in order parameter for methyls at the interface is actually slightly positive, reflecting steric restrictions to motion imposed by the proximity of the PBD46 ligand.

A large portion of the PBD46 binding surface on Cdc42Hs is composed of the β2 strand. When bound, PBD46 forms another β-strand along β2 such that the side chains of residues A41, V42, M45, and L46 point generally toward PBD46, whereas those of T43 and V44 point generally away from PBD46. The steric constraints imposed by PBD46 are reflected in the methyl side chain order parameters of residues in β2 (Figure 4, panel C): A41−T43 and L46 have relatively high order parameters in Cdc42Hs-PBD46, whereas those of V44 and M45 are relatively low. Thus, with the exceptions of T43 and M45, those methyl groups that will be near the incoming ligand are more flexible in the ligand-*free* state than those away from the incoming ligand [T43 evidently does not feel the effects of PBD46 as strongly as the other residues in β2, and high mobility is expected for methione methyl groups because of their large distance from the backbone (*44*)]. This is another indication that flexibility at the binding site is important prior to binding. Once PBD46 is bound, the order parameters of A41, V42, and L46 increase relative to the GMPPCP form, whereas those of T43−M45 decrease slightly (Figure 7, panel B).

While flexibility in the ligand-free form is important at the binding interface, regions away from the binding surface may be quite ordered. For example, all of the methyl side chains of the α4 helix (T141−L149) are characterized by order parameters greater than 0.8 in the ligand-free forms, indicating quite high order for side chains. However once PBD46 is bound, the order parameters drop dramatically to values ~0.5 except for those of A142 and A146 (Figure 4), indicating a significant increase in mobility in α4. The persistently high order parameters for the alanines in this region is unsurprising given that alanine methyls are strong reporters of backbone flexibility (*44*) and that the backbone remains well-ordered in this region upon PBD46 binding (*19*). Even so, *all* of the observed order parameters in α4 decrease relative to the GMPPCP form (Figure 7, panel B), illustrating the overall trend toward greater side chain flexibility away from the binding surface upon complex formation. It is interesting to note that K150, which is also far from the PBD46 binding region, has been used as a probe of PAK binding by observing a decrease in the fluorescence of a label placed on this residue (*4*, *45*). While the mechanism for this fluorescence reduction is not understood, it may be related to changes in the dynamics of residues in α4 such as those observed in this study.

Overall, the methyl groups exhibiting an increase in side chain mobility upon PBD46 binding are not restricted to a particular region of the protein but are largely in the hydrophobic core. This includes the residues in α4 described above as well as those residues in α3 that face α4. Likewise, methyl groups in α5 that interact with methyl groups in β5 and β6 (e.g., methyl groups of V168 in α5, V113 in β5, and V155 in β6) show increased mobility. This may simply reflect a slightly decreased packing of the hydrophobic core in the GMPPCP/PBD46-bound form. However, effects on the dynamics of residues far from the binding site are not unique to this study. Long-range effects have also been observed in NMR studies of protein−ligand interactions such as PBD46 binding to Cdc42Hs (backbone dynamics) (*19*) and interleukin 4 receptor binding to the phosphotyrosine binding domain of insulin receptor substrate 1 (*46*).

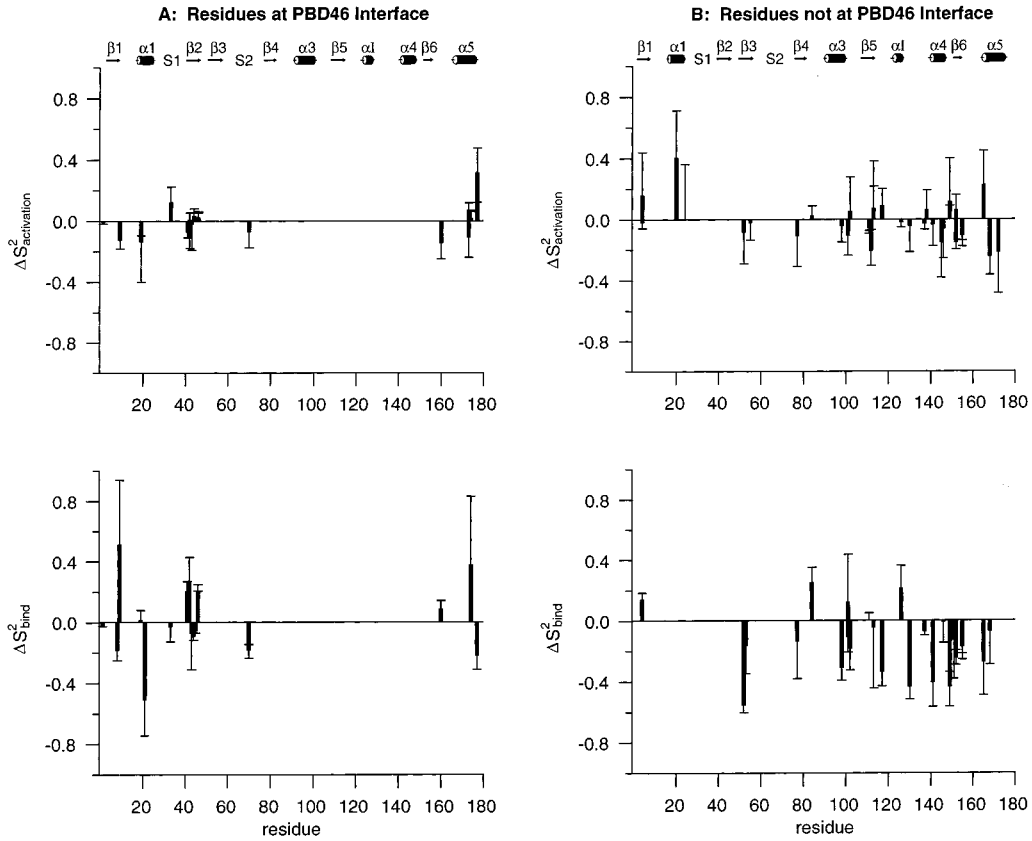

FIGURE 7: Effect of Cdc42Hs activation by GMPPCP (top) and binding of PBD46 (bottom) on the symmetry axis order parameters. (A) Residues on the PBD46 binding interface (within 5 Å of residues on PBD46). (B) Residues not on the PBD46 binding interface.

DISCUSSION

Balancing Entropy Losses Due to Substrate Binding. Binding of a substrate is necessarily accompanied by significant entropy losses for the system, due in part to restriction of motion at the protein−ligand interface. In the case of PBD46 binding, entropy losses also occur as the largely unstructured peptide folds into ordered structures and forms hydrogen bonds with Cdc42Hs. A significant reduction in the complexity of motion in the backbone was also observed upon binding of PBD46. For example, in the PBD46 form, 10 residues were fit with models that had fewer time scales than in the GMPPCP form, and 19 residues were fit with models that excluded the chemical exchange found in the GMPPCP form (*19*). This loss in motional complexity may provide an additional contribution to the decrease in entropy upon PBD46 binding. Some of these entropy losses are most likely offset by gains due to the exclusion of ordered water molecules from newly buried hydrophobic regions [i.e., the hydrophobic effect (*47*)]. However, we show in this study that an increase in the mobility of the side chains away from the PBD46 interface provides an additional mechanism for an increase in entropy, which helps to offset the entropy costs of ligand binding and drive the formation of the protein−ligand complex.

The various types of motions described by S^2_{axis} occur on a picosecond−nanosecond time scale (*12*). For alanine residues, the tetrahedral geometry of C^α restricts these motions largely to those contributed by the backbone. However, for all other methyl groups, torsional oscillations about the various χ angles are also relevant. Thus, the "expected" S^2_{axis} values for a given methyl group type tend to decrease as distance from the backbone increases (*44*). Nicholson et al. (*36*) have described the relationship between S^2_{axis} and a geometrical observable for three plausible types of internal motion for leucine methyls, assuming a rigid backbone: (i) diffusion of the $C^\delta-C^\gamma$ bond axis within a cone of semiangle θ_o, (ii) restricted rotational diffusion of the $C^\gamma-C^\beta$ bond axis within an angular range of $\pm\ \gamma_o$, and (iii) two site jump motion between the two populated rotamers of the $C^\delta-C^\gamma$ bond axis (differing by a rotation of 109.5°),[3] described by a relative population, *r*. This last model assumes that there are only two significantly populated rotamers about χ_1 and χ_2 (*48*, *49*), that there are no bond librations, and that the interconversion between the two rotameric states is fast on the NMR time scale (*50*, *51*). We have calculated the values of the appropriate parameter for each model for those leucine methyls that have rigid backbones (*19*) and are observed in both GDP and PBD46 forms (Table 3). These results indicate that in the diffusion in a cone or restricted rotational diffusion models, the decrease in S^2_{axis} is reflected in a significantly higher angular amplitude in the PBD46 form than in the GDP form. Alternatively, using the two-site jump model, increased flexibility in the PBD46 form is manifested by significant

[3] Since the NMR relaxation mechanisms are sensitive only to rotations and not to translations, only the change in orientation of the $C^\gamma-C^\delta$ bond vectors between the two rotameric states is relevant. Holding the $C^\alpha-C^\beta$ bond fixed in space, a conversion from one of these rotameric states to the other results in a dramatic change in the position of the $C^\gamma-C^\delta$ bond axis. If the initial and final $C^\gamma-C^\delta$ bonds are translated such that both C^γ atoms are placed at the origin of a common reference frame, the angle between the original and final bond vectors is 109.5°.

Table 3: Diffusion in a Cone, Restricted Rotational Diffusion and Two-Site Jump Descriptions of the Side Chain Motions of Leucine Resides in Inactive and Ligand-Bound Cdc42Hs[a]

	S^2_{axis}		θ_o (deg)[b]		γ_o (deg)[c]		r[d]	
residue[a]	GDP	PBD46	GDP	PBD46	GDP	PBD46	GDP	PBD46
L70	0.605	0.352, 0.361	33	45, 46	44	66, 67	0.22	0.66, 0.71
L79	0.839	0.388	20	44	26	63	0.07	0.55
L149	0.785, 0.812	0.496, 0.523	21, 23	37, 38	28, 30	50, 53	0.08, 0.09	0.30, 0.34
L160	0.424, 0.478	0.352, 0.424	39, 42	42, 46	55, 59	59, 67	0.336, 0.46	0.46, 0.71
L165	0.361	0.316	45	48	66	72	0.66	1
L174	0.605, 0.605	1.0	33, 33	0	44, 44	0.1	0.22, 0.22	0

[a] Only those leucine residues for which data were available for both GDP and PBD46 forms and which had rigid backbones ($S^2 > 0.9$ for amide $^{15}N-H$ bonds at residues i and i+1) (*19*) were considered. [b] Cone angle swept by $C^\delta-C^\gamma$ bond axis diffusion, obtained from the expression: $S^2_{axis} = [(\cos\theta_o(1 + \cos\theta_0)/2)]^2$ (*36*). [c] Angle swept by restricted rotational diffusion of $C^\gamma-C^\beta$ bond axis, obtained from the expression: $S^2_{axis} = (1/9)[1 + (8\sin^2\gamma_0(1 + 2\cos^2\gamma_0)/3\gamma_0^2)]$ (*36*). [d] Relative population of the two rotameric states of the $C^\delta-C^\gamma$ bond axis, obtained from the expression: $S^2_{axis} = 1 - (8/3)[(r/(1 + r)^2)]$. The two rotameric states interconvert by rotation about the $C^\delta-C^\gamma$ bond axis by 109.5°. The relative population r ranges from 0, when only one of the two states is populated, to 1, when both states are equally populated (*36*).

population of the second rotameric state. In the case of L174, which is on the PBD46 binding interface (*21*) and experiences a decrease in S^2_{axis}, all of the motional parameters *decrease* in magnitude. Because combinations of motions are likely to be present for a given residue, we view these motional models as limiting cases of the true amplitudes of motion. Thus, the observed decrease in the methyl side chain order parameters represents a composite of a variety of side chain motions that are in general larger in the PBD46 form than in the GDP or GMPPCP forms. Increases in backbone motion upon binding have been previously observed in proteins such as the mouse major urinary protein I upon binding of its small pheromone ligand (*14*) and in the 4-oxalocrotonate tautomerase enzyme upon interaction with its inhibitor (*52*). However, to our knowledge this is the only reported case of an observed increase in side chain motion upon substrate binding.

The approximate contribution of side chain entropy to the thermodynamics of PBD46 binding to Cdc42Hs were assessed by using the measured side chain order parameters to estimate changes in conformational entropy. The motions of the methyl group bond axes were described using a classical rotational partition function according to the treatment of Yang et al. (*16*). Because the assigned methyl groups in the PBD46-free (GMPPCP form) and PBD46-bound forms differ in some cases, and because the theory applies only to methyl groups with $S^2_{axis} < 0.95$, only 33 methyls could be compared directly. The estimated contribution to the entropy of PBD46 binding from the motions of this subset of side chains is $\Delta S_{bind,meth} \sim +18 \pm 7$ cal/mol·K, resulting in an entropic contribution to ΔG_{bind} of $T\Delta S_{bind,meth} \sim +5 \pm 2$ kcal/mol at 298 K. Although these methyls represent only a subset of all of the methyl groups in the protein, they sample virtually all regions of the protein and thus provide an estimate of the entropy effects due to a cross-section of side chain motions. However, it is important to note that the reported uncertainties are probably an underestimate of the actual errors in $T\Delta S_{bind,meth}$, as there are additional uncertainties arising from the assumptions in this treatment. However, the calculated entropic contribution to ΔG_{bind} cannot be attributed to the effects from anisotropic tumbling: if anisotropic motions of the ligand-free form[2] are taken into account, then the estimated entropic contribution to ΔG_{bind} from side chain motions becomes $T\Delta S_{bind,meth} \sim +8 \pm 5$ kcal/mol at 298 K, which is similar in magnitude and sign to the isotropic case.

The total entropic contribution to the free energy of binding can be estimated from the binding affinity, [K_d = 16 nM (*4*)], and the total enthalpy of binding [$\Delta H_{bind} = -13$ kcal/mol, from isothermal titration calorimetry (*53*)], to be approximately $T\Delta S_{bind} = -2.4$ kcal/mol at 298 K. While the estimations of side chain contributions to the total entropy of binding are limited to only methyl-bearing side chains, assuming that all motions are uncorrelated (and thus provide only an upper bound to $T\Delta S_{bind,meth}$) and are limited to events that occur on a picosecond−nanosecond time scale, it is clear that the entropic contributions from the increased side chain disorder are on the same order of magnitude as the total entropic contribution, and are in the direction to increase binding affinity.

As a comparison, we also considered the changes in side chain entropy due to nucleotide exchange, which are expected to be negligible due to the similarity of the side chain dynamics of the GDP and GMPPCP forms. On the basis of the order parameters for the 38 methyl groups observed in both the -GDP and -GMPPCP forms, $\Delta S_{ex,meth}$ was estimated to be $+2 \pm 10$ cal/mol·K, which results in an entropic contribution of $T\Delta S_{ex,meth} \sim +1 \pm 3$ kcal/mol at 298 K. As expected from the small change in the side chain order parameters upon activation, the entropic contributions to $\Delta G_{activation}$ from side chain motions are insignificant.

Other workers have sought to quantify the contributions from side chain motions to the overall free energy changes associated with events such as ligand binding. In a study of a calmodulin−peptide complex, Lee et al. (*12*) found that the motions of the side chains become more restricted upon complex formation, while the dynamics of the backbone remained unaffected by peptide binding. These authors calculated an overall value for $T\Delta G_{bind}$ of −35 kcal/mol at 35 °C, assuming that all side chains behave similarly to the observed methyl groups and that the backbone does not contribute to the overall entropy change. This negative entropic contribution represents a significant barrier to binding that is presumably overcome by highly favorable enthalpy changes. While it is unsurprising that different proteins achieve a negative free energy of binding by partitioning energy in different ways, and interesting that the side chains in Cdc42Hs and calmodulin behave quite differently, we suggest that caution be used in interpreting entropy changes based solely on order parameters. For example, while the backbone order parameters for Cdc42Hs also did not change appreciably upon ligand binding, the

number of time scales required to fit the relaxation data did change significantly (models with fewer time scales and less chemical exchange were sufficient for the PBD46 form in most cases) (*19*). Thus for Cdc42Hs, changes in backbone flexibility are manifested by changes in the time scales of motion rather than in the amplitudes of motion (i.e., order parameters). It is for this reason that contributions to the entropy of PBD46 binding could not be estimated with any accuracy from the backbone motions of Cdc42Hs.

Perhaps the most far-reaching conclusion from this study is the connection between protein flexibility and function. Regions of Cdc42Hs that are involved in molecular recognition are more flexible than those regions that are not involved in molecular recognition. While some of these regions may actually be fairly disordered (i.e., switch I and portions of switch II), some are quite well structured (i.e., β2). Different types and extents of flexibility presumably allow the protein and ligand to achieve an induced fit upon binding, reducing the overall energy costs by maintaining a higher entropy and increasing the probability of docking in a favorable arrangement. This ability to induce a fit in a flexible region is evident from the fact that several different proteins [GDI (*3*), GAP (*1*, *2*), and several kinases (*4*−*6*)] interact with Cdc42Hs at the same flexible locations in the molecule (switch I and switch II). The connection between flexibility and activity for particular regions of proteins has also been observed in a wide variety of other systems [see also Forman-Kay (*11*)]. In one of the first ^{2}H relaxation studies of side chain dynamics, Kay, et al. (*54*) found that regions of the C-terminal SH2 domain of phospholipase C-γ1 (PLCC SH2) that interact with a peptide ligand have high mobility in both complexed and uncomplexed forms. Lee et al. (*12*) have also found that the largest changes in methyl side chain order parameters upon calmodulin−peptide complex formation occurred at the binding interface. In a study of the backbone dynamics of the basic leucine zipper of GCN4, Bracken et al. (*13*) found that the region of the protein that interacts with DNA is more disordered than the remainder of the protein. Motions that occur on longer time scales than those described using order parameters (∼picosecond−nanosecond) are also important, as demonstrated by Feher and Cavanagh (*8*), who showed that regions of the SpoOF protein backbone that experience motions on the millisecond time scale are critical for protein−protein interactions.

In conclusion, we have found that regions of Cdc42Hs that are involved in protein−protein interactions exhibit backbone and side chain dynamics characteristics that are distinct from those in the remainder of the protein. Furthermore, binding of the effector fragment PBD46 is accompanied by a loss in backbone mobility (*19*) and an increase in methyl side chain flexibility. Although only a subset of side chains were examined, the estimated increase in entropy in the side chains appears to be of the same order of magnitude as the overall entropic contribution to the free energy of binding. It is evident that backbone and side chain motions play an extremely important role in molecular recognition and that an understanding of not only protein structure, but also of protein flexibility is crucial for a complete understanding of the mechanism of protein function.

ACKNOWLEDGMENT

We thank the Laboratory of Chemical Physics at the National Institutes of Health and Drs. Dan Garrett and Frank Delaglio for making available the programs PIPP and NMRPipe which were useful in analyzing our NMR data. We thank Rob McFeeters, Jeffrey Reinking, Chunyu Wang, Michael Sutcliffe, Richard Cerione, Greg Weiland, Nicolas Nassar, and Dawit Gizachew for helpful discussions.

REFERENCES

1. Rittinger, K., Walker, P. A., Eccleston, J. F., Nurmahomed, K., Owen, D., Laue, E., Gamblin, S. J., and Smerdon, S. J. (1997) *Nature 388*, 693−607.
2. Nassar, N., Hoffman, G. R., Manor, D., Clardy, J. C., and Cerione, R. A. (1998) *Nat. Struct. Biol. 5*, 1047−1052.
3. Hoffman, G. R., Nassar, N., and Cerione, R. A. (2000) *Cell 100*, 345−356.
4. Guo, W., Sutcliffe, M. J., Cerione, R. A., and Oswald, R. E. (1998) *Biochemistry 37*, 14030−14037.
5. Abdul-Manan, N., Aghazadeh, B., Liu, G. A., Majumdar, A., Ouerfelli, O., Siminovitch, K. A., and Rosen, M. K. (1999) *Nature 399*, 379−383.
6. Mott, H. R., Owen, D., Nietlispach, D., Lowe, P. N., Manser, E., Lim, L., and Laue, E. D. (1999) *Nature 399*, 384−388.
7. Stock, A. (1999) *Nature 400*, 221−222.
8. Feher, V. A., and Cavanagh, J. (1999) *Nature 400*, 289−293.
9. Rasmussen, B. F., Stock, A. M., Ringe, D., and Petsko, G. A. (1992) *Nature 357*, 423−424.
10. Clackson, T., and Wells, J. A. (1995) *Science 267*, 383−386.
11. Forman-Kay, J. D. (1999) *Nat. Struct. Biol. 6*, 1086−1087.
12. Lee, A. L., Kinnear, S. A., and Wand, A. J. (2000) *Nat. Struct. Biol. 7*, 72−77.
13. Bracken, C., Carr, P., A., Cavanagh, J., and Palmer, A. G., III (1999) *J. Mol. Biol. 285*, 2133−2145.
14. Zidek, L., Novotny, M. V., and Stone, M. J. (1999) *Nat. Struct. Biol. 6*, 1118−1121.
15. Doig, A. J., and Sternberg, J. E. (1995) *Protein Sci. 4*, 2247−2251.
16. Yang, D., and Kay, L. E. (1996) *J. Mol. Biol. 263*, 369−382.
17. Karplus, M., and Kuschick, J. N. (1981) *Macromolecules 14*, 325−332.
18. Li, Z., Raychaudhuri, S., and Wand, J. A. (1996) *Protein Sci. 5*, 2647−2650.
19. Loh, A. P., Guo, W., Nicholson, L., and Oswald, R. E. (1999) *Biochemistry 38*, 12547−12557.
20. Bourne, H. R., Sanders, D. A., and McCormick, F. (1991) *Nature 349*, 117−127.
21. Gizachew, D., Guo, W., Chohan, K. K., Sutcliffe, M. J., and Oswald, R. E. (2000) *Biochemistry 39*, 3963−3971.
22. Hirshberg, M., Stockley, R. W., Dodson, G., and Webb, M. R. (1997) *Nat. Struct. Biol. 4*, 147−152.
23. Kraulis, P. J., Domaille, P. J., Campbell-Burk, S. L., VanAken, T., and Laue, E. D. (1994) *Biochemistry 33*, 3515−3531.
24. Milburn, M. V., Tong, L., DeVos, A. M., Brunger, A., Yamaizumi, Z., Nishimura, S., and Kim, H. (1990) *Science 247*, 939−945.
25. Wei, Y., Zhang, Y., Derewenda, U., Liu, X., Minor, W., Nakamoto, R. K., Somlyo, A. V., Somlyo, A. P., and Derewenda, Z. S. (1997) *Nat. Struct. Biol. 4*, 699−703.
26. Feltham, J. L., Dötsch, V., Raza, S., Manor, D., Cerione, R. A., Sutcliffe, M. J., Wagner, G., and Oswald, R. E. (1997) *Biochemistry 36*, 8755−8766.
27. Yamazaki, T., Lee, W., Arrowsmith, C. H., Muhandiram, D. R., and Kay, L. E. (1994) *J. Am. Chem. Soc. 116*, 11655−11666.
28. John, J., Sohmen, R., Feurstein, J., Linke, R., Wittinghofer, A., and Goody, R. S. (1990) *Biochemistry 29*, 6058−6065.
29. Muhandiram, D. R., Yamazaki, T., Sykes, B. D., and Kay, L. E. (1995) *J. Am. Chem. Soc. 117*, 11536−11544.

30. Marion, D., Driscoll, P. C., Kay, L. E., Wingfield, P. T., Bax, A., Gronenborn, A., and Clore, G. M. (1989) *Biochemistry 28*, 6150−6156.
31. Delaglio, F., Grzeseik, S., Vuister, G., Zhu, G., Pfeifer, J., and Bax, A. (1995) *J. Biomol. NMR 6*, 277−293.
32. Garrett, D. S., Powers, R., Gronenborn, A. M., and Clore, G. M. (1991) *J. Magn. Reson. 95*, 214−220.
33. Nicholson, L. K., Grzesiek, S., Yamazaki, T., Stahl, S. J., Kaufman, P. T., Wingfield, P. T., Domaille, P. J., Bax, A., and Torchia, D. A. (1995) *Nat. Struct. Biol. 2*, 274−280.
34. Lipari, G., and Szabo, A. (1982) *J. Am. Chem. Soc. 104*, 4546−4559.
35. Lipari, G., and Szabo, A. (1982) *J. Am. Chem. Soc. 104*, 4559−4570.
36. Nicholson, L. K., Kay, L. E., Baldisseri, D. M., Arango, J., Young, P. E., Bax, A., and Torchia, D. A. (1992) *Biochemistry 31*, 5253−5263.
37. Abragam, A. *Principles of Nuclear Magnetism* (1961) pp 264−353, Clarendon Press, Oxford.
38. Burnett, L. H., and Muller, B. H. (1971) *J. Chem. Phys. 55*, 5829.
39. Palmer, A. (1998) *ModelFree 4.0*, http://cpmcnet.columbia.edu/dept/gsas/biochem/labs/palmer
40. Hubbard, S. J., and Thornton, J. M. (1993) 'NACCESS', Computer Program, University College, Department of Biochemistry & Molecular Biology, London.
41. Tjandra, N., Feller, S. E., Pastor, R. W., and Bax, A. (1995) *J. Am. Chem. Soc. 117*, 12562−12566.
42. Tjandra, N., Wingfield, P., Stahl, S., and Bax, A. (1996) *J. Biomol. NMR 8*, 273−84.
43. Zheng, Z., Czaplicki, J., and Jardetzky, O. (1995) *Biochemistry 34*, 5212−5223.
44. Mittermaier, A., Kay, L. E., and Forman-Kay, J. D. (1999) *J. Biomol. NMR 13*, 181−185.
45. Leonard, D. A., Satoskar, R. S., Wu, W. J., Bagrodia, S., Cerione, R. A., and Manor, D. (1997) *Biochemistry 36*, 1173−1180.
46. Olejniczak, E. T., Zhou, M.-M., and Fesik, S. W. (1997) *Biochemistry 36*, 4118−4124.
47. Tanford, C. (1973) *The Hydrophobic Effect*, Wiley, New York.
48. Benedetti, C. (1977) in *Proceedings of the Fifth American Peptide Symposium* (Goodman, M., Meienhofer, J., Eds.) pp 257−274, Wiley, New York.
49. Janin, J., Wodak, S., Levitt, M., and Maigret, B. (1978) *J. Mol. Biol. 125*, 357.
50. Batchelder, L. S., Sullivan, C. E., Jelinski, L. W., and Torchia, D. A. (1982) *Proc. Natl. Acad. Sci., U.S.A. 79*, 386.
51. Colnago, L. A., Valentine, K. G., and Opella, S. J. (1987) *Biochemistry 26*, 847.
52. Stivers, J. T., Abeygunawardana, C., Mildvan, A. S., and Whitman, C. P. (1996) *Biochemistry 35*, 16036−16047.
53. Guo, W. (1999) Ph.D., Cornell University.
54. Kay, L. E., Muhandiram, D. R., Farrow, N. A., Aubin, Y., and Forman-Kay, J. D. (1996) *Biochemistry 35*, 361−368.
55. Guex, N., and Pietsch, M. C. (1997) *Electrophoresis 18*, 2714−2723, http://www.expasy.ch/spdbv/
56. Barton, G. J. (1993) *Prot. Eng. 6*, 37−40.
57. Bodenhausen, G., and Ruben, D. J. (1980) *Chem. Phys. Lett. 69*, 185−189.

BI002418F